International Journal of Microwave and Wireless Technologies

cambridge.org/mrf

A low-profile circularly polarized microstrip antenna using elliptical electromagnetic band gap structure

Shilpee Patil[1], Alka Verma[2], Anil Kumar Singh[3], Binod Kumar Kanaujia[4] and Suresh Kumar[5]

[1]Department of Electronics and Communication Engineering, Noida Institute of Engineering and Technology, Greater Noida, Uttar Pradesh, India; [2]Electronics Engineering, A.K.T.U., Lucknow, Uttar Pradesh, India; [3]Department of Electronics and Instrumentation Engineering, F.E.T., M.J.P. Rohilkhand University, Bareilly, Uttar Pradesh 243006, India; [4]School of Computational and Integrative Sciences, Jawaharlal Nehru University, New Delhi, India and [5]Department of Computer Science and Engineering, Netaji Subhas University of Technology, East Campus, Delhi, India

Research Paper

Cite this article: Patil S, Verma A, Kumar Singh A, Kanaujia BK, Kumar S (2022). A low-profile circularly polarized microstrip antenna using elliptical electromagnetic band gap structure. *International Journal of Microwave and Wireless Technologies* **14**, 1009–1018. https://doi.org/10.1017/S1759078721001367

Received: 5 January 2021
Revised: 29 August 2021
Accepted: 4 September 2021
First published online: 28 September 2021

Key words:
Axial ratio; bandwidth; elliptical electromagnetic band gap structure; slot

Author for correspondence:
Alka Verma,
E-mail: alkasinghmail@rediffmail.com

Abstract

This study investigates a low-profile circularly polarized (CP) antenna using coplanar waveguide feeding. Rectangular-shaped slots and an inverted L-shaped slit are entrenched into the ground plane to enhance the impedance bandwidth of the antenna. Furthermore, the antenna is implemented with six elliptical electromagnetic band gap structures on its substrate to enhance the −10 dB return loss bandwidth and also to generate CP waves. The experimental and theoretical results closely match each other and indicate that a simple and compact design antenna with dimensions of $0.317\lambda_0 \times 0.317\lambda_0 \times 0.023\lambda_0$($\lambda_0$ is the operating wavelength at 4.74 GHz in free space) achieves 36.9% (3.91–5.68 GHz) of the −10 dB return loss bandwidth and 9.98% (4.09–4.52 GHz) of the 3-dB axial ratio bandwidth, thus making it a favorable entrant for radio altimeter and wireless avionics infra-communication systems.

Introduction

In the present scenario in the field of technology, polarization plays a vital role in the proper functioning of communication systems because it allows the reception of signals irrespective of the alignment of the transmitting antennas. The attractive features of circularly polarized (CP) antennas, which includes their ability to overcome multi-path interferences and reduce the effect of Faraday rotation, make them very desirable in wireless communication systems. Several ways have been explored by various researchers to design a low-profile, cheap, and highly compact CP antenna; these methods include using a substrate of a high-dielectric constant [1, 2], implementing slots [3, 4] and slits [5, 6] on the patch, employing the ground plane with defective ground structures [7, 8], implementing reactive impedance surfaces (RISs) [9], using split-ring resonators [10], complementary split-ring resonators [11], etc. Although the aforementioned methods led to the miniaturization of the antenna, they also degraded the antenna performance due to the presence of surface wave propagation in the substrate of the antenna. To overcome the stated drawbacks, researchers proposed electromagnetic band gap (EBG) structures which are periodic/aperiodic metallic/dielectric structures that prohibit the surface waves from traveling in the substrate of the antenna by introducing a specified stop band, thus leading to an improved performance of the antenna. Many researchers have implemented such structures on the antenna's ground surface [12], on its substrate [13], by surrounding it around the patch [14], and also by using it as metasurface [15] and, thus, recuperated the antenna's performance. In [16], mushroom-shaped EBG structures were implemented on the ground plane and, by utilizing its polarization-dependent in-phase reflection property with a dipole antenna placed above it, was able to generate CP waves at 3.56 GHz with an improved performance but with the limitation of a large ground plane of size 100 mm × 100 mm. In [17], the performance of the CP antenna was improved by using an array of annular ring EBGs on the ground plane. Also, it achieved 10% reduction in the center frequency when compared to the antenna without EBG. Even though the structure proposed above showed an immense enhancement in terms of gain and efficiency, it still lacked compactness in terms of its physical dimensions. In [18], the CP waves were obtained using three N slots on the patch antenna and, later, on circular air hole as EBG structures were drilled on the substrate to enhance its performance and also to achieve compactness. However, it resulted in a complex fabrication process. In [19], a compact CP antenna at 1.57 GHz was presented by printing fractal EBG on the substrate of the antenna which is made from organic material. Nevertheless, the aforementioned proposed structure showed a

© The Author(s), 2021. Published by Cambridge University Press in association with the European Microwave Association

CAMBRIDGE UNIVERSITY PRESS

small axial ratio (AR) bandwidth of 31 MHz. In [20], a slot-loaded slot antenna with mushroom-shaped EBG cells around it was able to generate CP waves with wide AR bandwidth. In [21], CP radiation was generated with enhanced gain and CP bandwidth by placing an EBG array as a polarizer above a patch antenna. In [22], a CP array antenna was proposed by utilizing the polarization conversion property of EBG. Although this antenna achieved wide AR bandwidth and radar cross-section reduction, it eventually lacked miniaturization. In [23], polarization-dependent EBG structures were constructed to surround a rotated truncated patch in an attempt to design a CP antenna that would obtain an AR bandwidth of 50 MHz and a return loss bandwidth of 120 GHz. However, this led to an increase of the overall size of the antenna. In [24], a high-gain compact CP slot antenna at 5.1 GHz was proposed with hexagonal ring-shaped EBG on the substrate with an impedance bandwidth of 18%. Recently, EBGs have been implemented as metasurfaces [25, 26] to enhance the performance of CP antennas. In [27], a metasurface with a 4 × 4 square patch was designed to obtain a low-profile CP antenna. Although it achieved wide AR bandwidth, it achieved a narrow impedance bandwidth of 17%. A CP antenna, implemented with square-based metasurface, was proposed in [28]. It had a multiple-slit feeding structure and was able to achieve 17.3% of 3-dB gain bandwidth but faced complexity in fabrication. In [29], a coplanar waveguide (CPW)-fed CP antenna which had an inclined slot in the ground surface and was loaded with an EBG-based metasurface showed improved performance but lacked compactness. In [30], an EBG array was implemented as a partially reflective surface above a metamaterial CP antenna to enhance its directivity but led to an increase in the physical size of the antenna. In [31], a broadband spiral CP antenna was designed using planar EBG. It achieved a wide AR bandwidth by lengthening the concentric-shaped EBG patches but led to the lowering of gain at a high-frequency range. Thus, the above reported EBG-based CP antennas either lacked compactness or were not able to show wide return loss bandwidth or axial ratio bandwidth. With the aim of achieving a CP antenna and to show improvement in terms of impedance bandwidth and AR bandwidth along with miniaturization in size, in this paper, we have proposed a CPW-fed patch antenna with modified ground plane and six ellipse-shaped EBGs on the bottom side of the substrate to achieve miniaturization as well to report wide impedance and AR bandwidth. The proposed antenna is applicable for radio altimeter and wireless avionics infra-communication (WAIC) systems.

Proposed antenna configuration and ellipse-shaped electromagnetic band gap (EEBG) design

Design and evolution stages of proposed antenna

Figure 1 depicts the proposed antenna which comprises the patch with CPW feed built on an FR-4 substrate of thickness h and having a dielectric constant of 4.4. The ground plane has dimensions of $L_g \times W_g$, is modified with rectangular slots and inverted L slit, and the substrate is etched with six EEBG structures at its bottom. Table 1 depicts the optimized parameters of the proposed structure. The suggested antenna is able to generate a wide impedance bandwidth with improved axial ratio bandwidth and gain by implementing the EEBG on its substrate. The three steps in which the design of the proposed antenna evolved are shown in Fig. 2. Step 2(a) illustrates a CPW-fed patch antenna (antenna A)

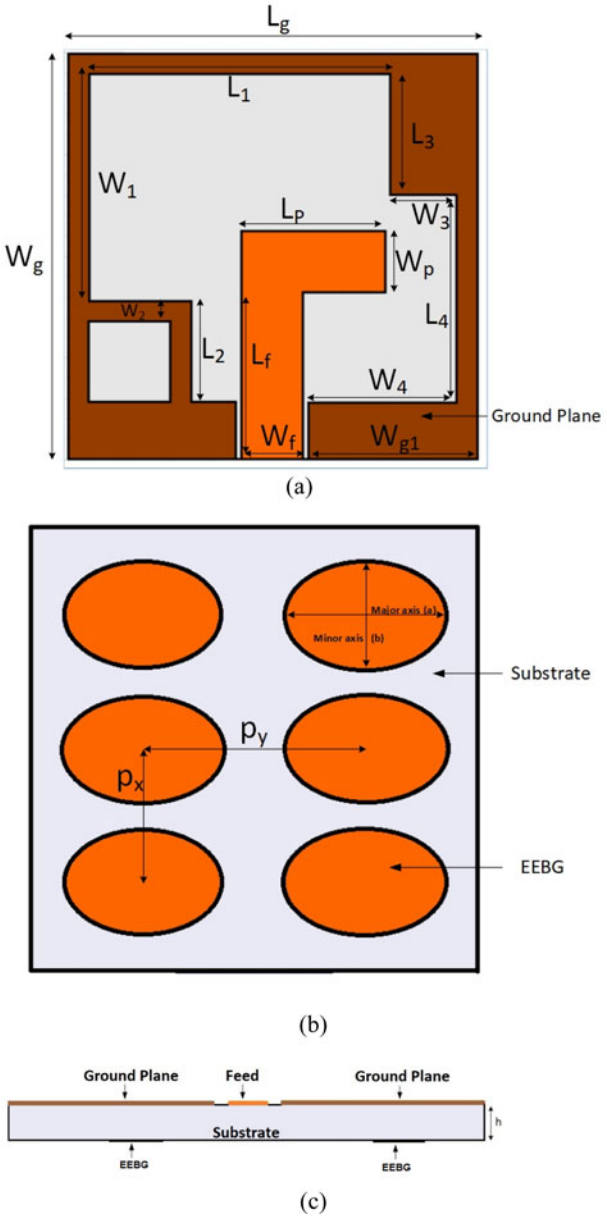


Fig. 1. Proposed antenna: (a) top view, (b) bottom view, and (c) side view.

with a rectangular slot of dimensions $L_s = 18$ mm and $W_s = 16.2$ mm. Figure 3 depicts the S_{11} response of antenna A, which illustrates that an impedance bandwidth of 26.9% (4.05–5.31 GHz) is obtained when linearly polarized waves are generated, as shown in Fig. 4. Moreover, as depicted in Fig. 5, the peak gain of antenna A is 0.18 dBic in the operating bandwidth and is negative in the higher frequency range. To improve the impedance bandwidth and gain, the ground plane is further modified with a rectangular slit ($L_3 \times W_3$) on the top right corner and inverted L-shaped slit of length L_2 and width W_2 are placed on the bottom right side of the ground plane. As shown in Fig. 3, the impedance bandwidth increases to 31% (3.90–5.33 GHz) and, as depicted in Fig. 5, the gain improves to 1.2 dBic. It is also observed from Fig. 4 that no CP waves are present. For the generation of CP waves, the dimensions of EEBG unit cell and the periodicity in the x and y axes are adjusted such that the impedance along the two diagonal directions vary, causing the induced current to change and results in the

https://doi.org/10.1017/S1759078721001367 Published online by Cambridge University Press

Table 1. Parameters of the proposed antenna

Parameters	L_g	W_g	W_{g1}	h	L_f	W_f	L_p	W_p	L_s
Value (mm)	20	20	8.25	1.5	11.25	3.0	7.0	3.0	18
Parameters	L_1	W_1	L_2	W_2	L_3	W_3	L_4	W_4	W_s
Value (mm)	14.75	11.2	5.0	1.0	6.0	3.25	10.2	7.25	16.2

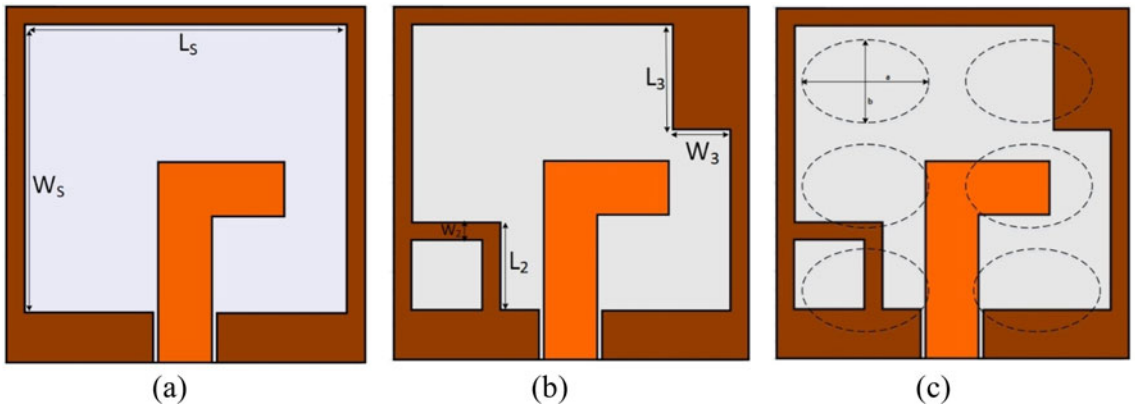


Fig. 2. Evolution steps of proposed antenna: (a) antenna A, (b) antenna B, and (c) antenna C (proposed antenna).

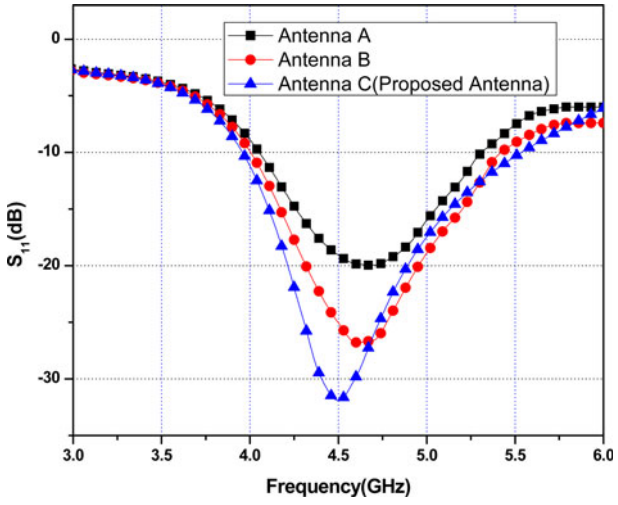


Fig. 3. Simulated S_{11} varying with frequency of antennas A, B, and C.

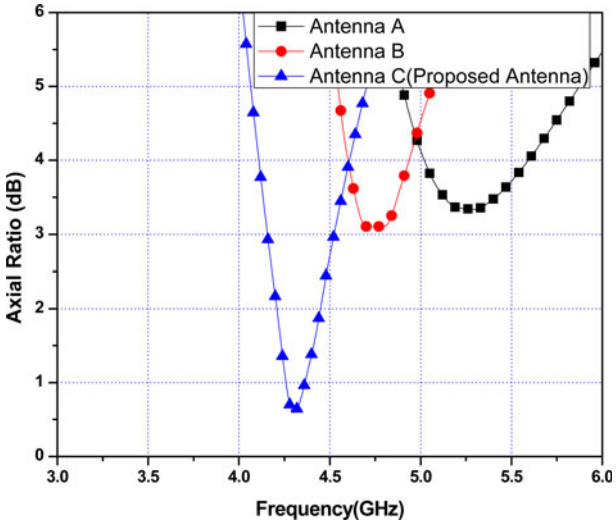


Fig. 4. Simulated axial ratio varying with frequency of antennas A, B, and C.

two orthogonal components to change as well. Thus, by optimizing the parameters of EEBG, when the condition $|Z_1| = |Z_2|$ and $\text{ang}(Z_1 - Z_2) = \pm 90°$ is achieved, the CP radiation is obtained. Therefore, it is observed from Fig. 4 that antennas A and B were unable to obtain CP radiation but, by implementing six EEBGs on the bottom of the substrate, antenna C resulted in 3 dB AR bandwidth of 8.53% (4.15–4.52 GHz) due to the generation of two orthogonal modes with a phase of 90°. It is also depicted from Fig. 3 that antenna C shows an improvement in impedance bandwidth of 33.33% (3.95–5.53 GHz) from 31% (3.90–5.33 GHz) of antenna B. Furthermore, due to additional inductance and capacitance introduced because of the elliptical-shaped EBG, there is a shift in the impedance bandwidth toward the lower frequency region. As depicted in Fig. 5, the EEBG inhibits the propagation of surface waves resulting in the gain of antenna C to enhance the peak gain to 3.13 dBic in the operating bandwidth (Table 2).

EEBG unit cell design

An EEBG which consists of six ellipse-shaped metal plates, arranged in the 3 × 2 layout with periodicity in the x and y directions as p_x and p_y, respectively, is proposed. It is placed on the antenna's bottom surface of the substrate, which is made of FR4 having thickness h. The elliptical EBG axes comprising of minor axis and major axis are situated at $a = 4.8$ mm in the x direction and with $b = 7.2$ mm in the y direction, respectively. Table 3 lists the optimized dimensions of the EEBG.

https://doi.org/10.1017/S1759078721001367 Published online by Cambridge University Press

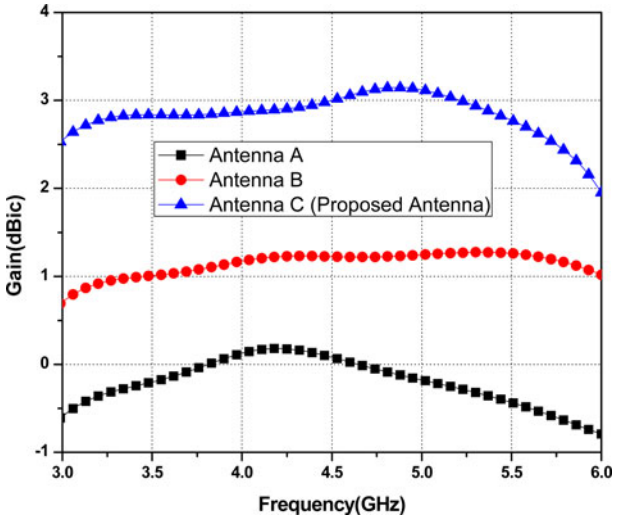


Fig. 5. Simulated Gain varying with frequency of antenna A, B and C.

Using Ansoft's High Frequency Simulator Software (HFSS) version 15, the unit cell of the proposed EEBG is simulated and its in-phase reflection properties [32] are analyzed by implementing the Floquet-port model [33]. It is observed in Fig. 6 that at 4.48 GHz, 0° reflection phase is obtained and, in the frequency range of 2.32–6.13 GHz, the phase varies from +90° to −90°, indicating that the frequency band gap of the proposed EBG concurs to the operating bandwidth of our proposed antenna.

Figure 7 depicts the equivalent circuit diagram of the unit cell EEBG, which is shown as the LC resonant circuit [33], where C is the capacitance between the adjacent elliptical shape EBG unit cell and L is the inductance that occurs due to the perfect electric conductor-backed substrate whose thickness is not more than a quarter wavelength of the preferred frequency. Equations (1) and (2) display the equivalent input impedance (Z_0) and the resonant frequency (f_0) of the unit cell EEBG:

$$Z_0(\omega) = \frac{j\omega L}{1 - \omega^2 LC} \tag{1}$$

$$f_0 = \frac{1}{2\pi}\sqrt{\frac{1}{L\,C}} \tag{2}$$

Parametric analysis

To obtain the final dimensions of the proposed antenna, parametric analysis was performed by varying the different parameters of the proposed antenna. This included the ratio of the major to minor axes of EEBG, its periodicity on both x and y directions, the length and width of the CPW feed, etc.

Table 3. Optimized dimensions of EEBG

Sl. no.	EEBG parameters	Dimensions (mm)
1	Minor axes of ellipse, a	4.8
2	Major axes of ellipse, b	7.2
3	Ratio of major to minor axes of ellipse, X_e	1.5
4	Periodicity in x direction, p_x	6
5	Periodicity in y direction, p_y	10

Parametric study on varying the ratio of major to minor axes EEBG, X_e

Figure 8 portrays that on varying the value of X_e from 1.4 to 1.6 mm, X_e affects both the impedance bandwidth as well as the axial ratio bandwidth. As observed in Fig. 8, S_{11} significantly degrades to −26.4 dB when X_e is 1.4 mm. On increasing the value of X_e to 1.5 mm, it is found that S_{11} improves significantly to −32 dB. However, when the X_e is set at 1.6 mm, the S_{11} degrades to −30.5 dB. Moreover, the AR in dB at 1.5 mm is 0.61, which is the lowest when compared to 0.71 and 1.51 dB at 1.6 and 1.4 mm, respectively. Hence, it can be deduced that better impedance matching followed by a good AR value resulted in the value of X_e to be optimized to 1.5 mm.

Parametric study on the periodicity along x axis of EEBG, p_x

It is illustrated in Fig. 9 that upon varying the periodicity (p_x) along the x direction, at 6 mm, the resonant frequency shifts to the lower side of 4.49 GHz with the value of S_{11} being −31.99 dB, which is better in comparison with −19 dB at 7 mm and −29.9 dB at 5 mm. Moreover, an axial ratio value of 0.55 dB at 6 mm with an improved AR bandwidth of 370 MHz in comparison with the AR value of 2.18 and 2.64 dB at 7 and 5 mm, respectively, leads to the finalization of the value of p_x to 6 mm.

Parametric study on varying the periodicity along y axis of EEBG, p_y

Figure 10 depicts that upon increasing the periodicity (p_y) in the y direction, the impedance bandwidth decreases to 1500 MHz at 11 mm, with the value of AR also decreasing to 1.86 dB. At 10 mm, the resonant frequency shifts to the lower side, with the value of the impedance bandwidth increasing to 1580 MHz along with an

Table 2. Parameters of different design configurations

Parameters	Antenna A	Antenna B	Antenna C (proposed antenna)
Impedance bandwidth (MHz)	1260	1430	1580
Axial ratio bandwidth (MHz)	–	–	370
Peak gain (dBic) in the operating bandwidth	0.18	1.26	3.13
Peak gain (dBic) in the CP bandwidth	–	–	3.0

https://doi.org/10.1017/S1759078721001367 Published online by Cambridge University Press

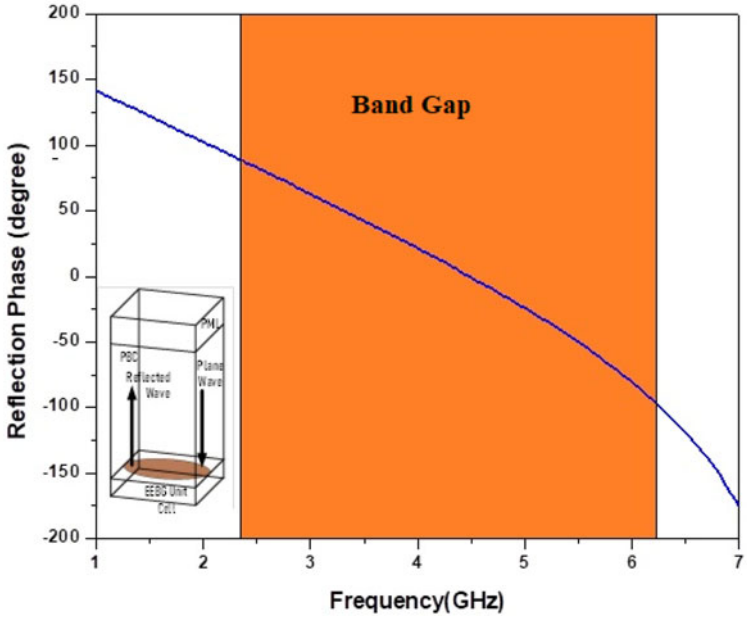


Fig. 6. Reflection phase diagram of the proposed unit cell EEBG (inset view: unit cell model).

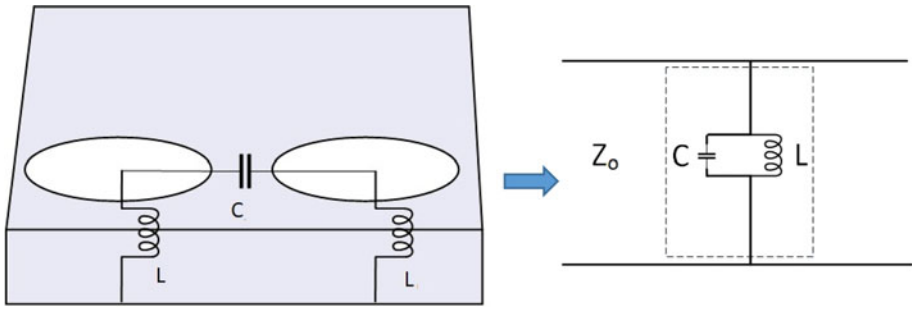


Fig. 7. Equivalent circuit diagram of the proposed unit cell EEBG.

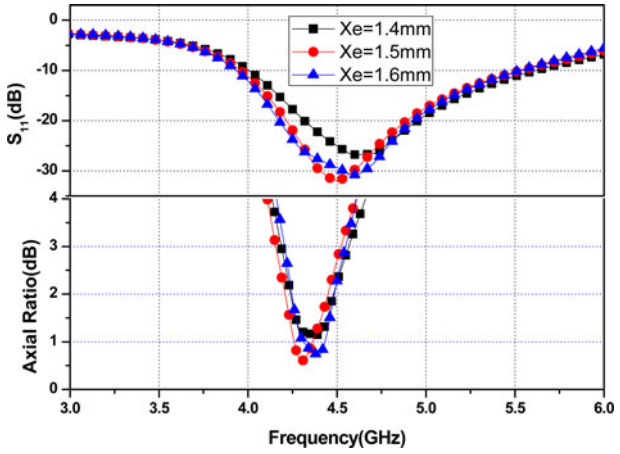


Fig. 8. Effect on varying X_e with frequency on S_{11} (simulated) and axial ratio (simulated).

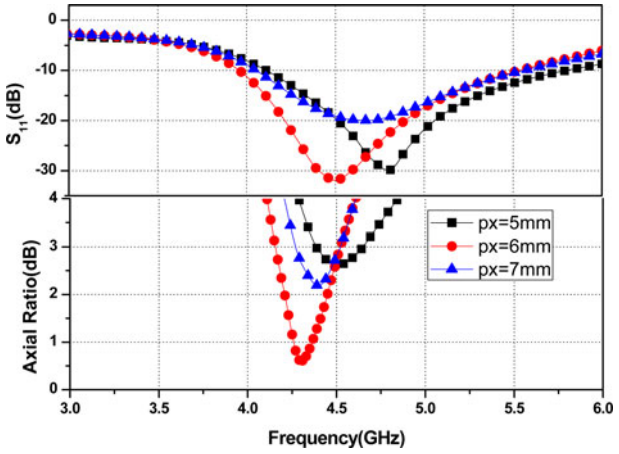


Fig. 9. Effect on varying p_x with frequency on S_{11} (simulated) and axial ratio (simulated).

improvement of the axial ratio value to 0.55 dB, as compared to 0.99 and 1.86 dB at 9 and 11 mm, respectively.

Parametric study on varying the width of feed, W_f

By varying the width of the CPW feed, the resonant frequency of the antenna shifts to the lower side to 4.49 GHz at 3 mm, as observed in Fig. 11. Again upon increasing W_f to 3.1 mm, the resonant frequency shifts to the higher side of 4.74 GHz with a very poor AR value of 1.06 dB. It is also observed that when the value of W_f is 3 mm, the value of AR is 0.55 dB, which is better in comparison with 1.06 and 2.89 dB at 3.1 and 2.9 mm, respectively. Thus, the value of W_f is optimized to 3 mm.

https://doi.org/10.1017/S1759078721001367 Published online by Cambridge University Press

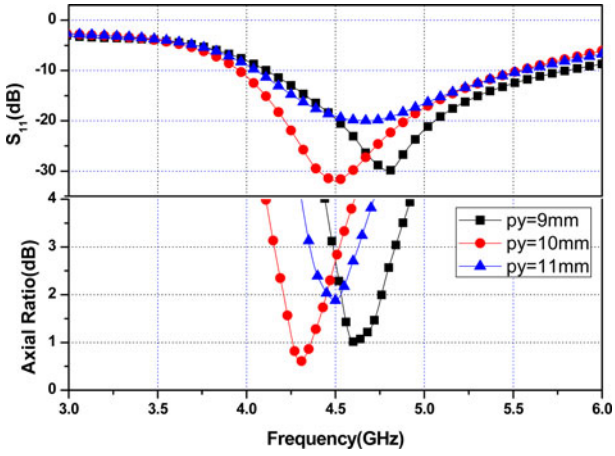


Fig. 10. Effect on varying p_y with frequency on S_{11} (simulated) and axial ratio (simulated).

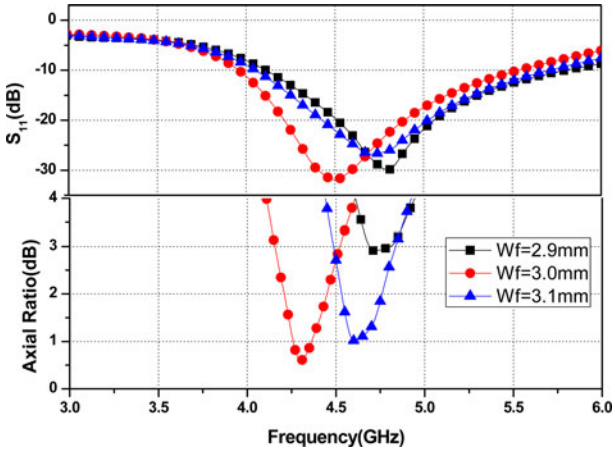


Fig. 11. Effect on varying W_f with frequency on S_{11} (simulated) and axial ratio (simulated).

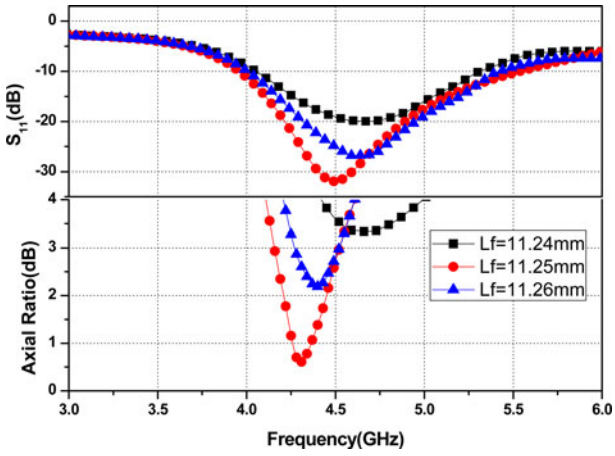


Fig. 12. Effect on varying L_f with frequency on S_{11} (simulated) and axial ratio (simulated).

Parametric study on varying the length of feed, L_f

As depicted in Fig. 12, the effect of the length of antenna feed on S_{11} and AR is observed by varying the value of L_f from 11.24 to 11.26 mm in steps of 0.01 mm. The simulated results from Fig. 12 indicate that as the value of L_f increases, the resonance frequency of the antenna shifts to the lower side with the lowest being 4.95 GHz when the L_f is equal to 11.25 mm. Nevertheless, it is also depicted in Fig. 12 that upon increasing the value of L_f, the AR characteristics of the antenna are affected. When the L_f equals 11.24 mm, the value of AR deteriorates below 3 dB. The minimum value of AR is obtained at 4.3 GHz; this corresponds to the value of L_f being equal to 11.25 and degrades further as the L_f increases to 11.26 mm. Hence, the value of L_f is optimized to 11.25 mm.

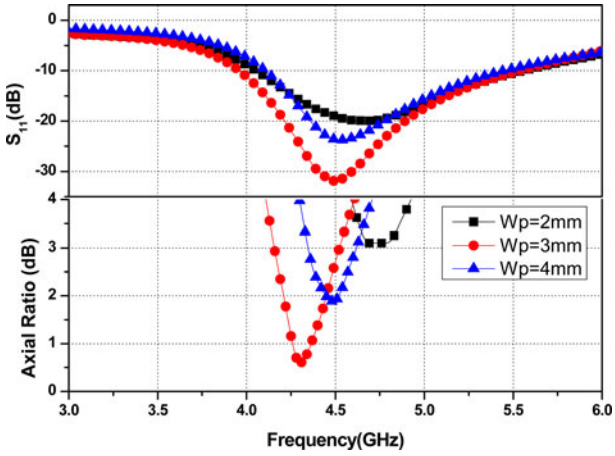


Fig. 13. Effect on varying W_p with frequency on S_{11} (simulated) and axial ratio (simulated).

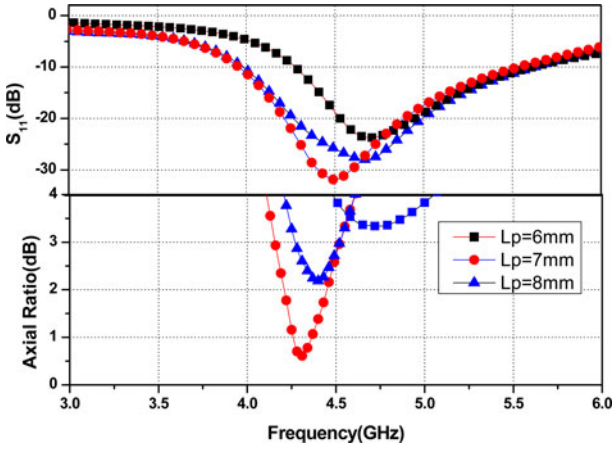


Fig. 14. Effect on varying L_p with frequency on S_{11} (simulated) and axial ratio (simulated).

Parametric study on varying the width of patch, W_p

As depicted in Fig. 13, by varying the patch width at 2, 3, and 4 mm, S_{11} attains the value of −20, −24, and −31.4 dB, respectively, indicating that better impedance matching is obtained when W_p is 3 mm. Moreover, the effect on increasing the patch width of the antenna results in the degradation of the AR characteristic, thus showing poor AR of 3.1 and 1.81 dB when the W_p equals 2 and 3 mm, respectively. The minimum value of AR,

https://doi.org/10.1017/S1759078721001367 Published online by Cambridge University Press

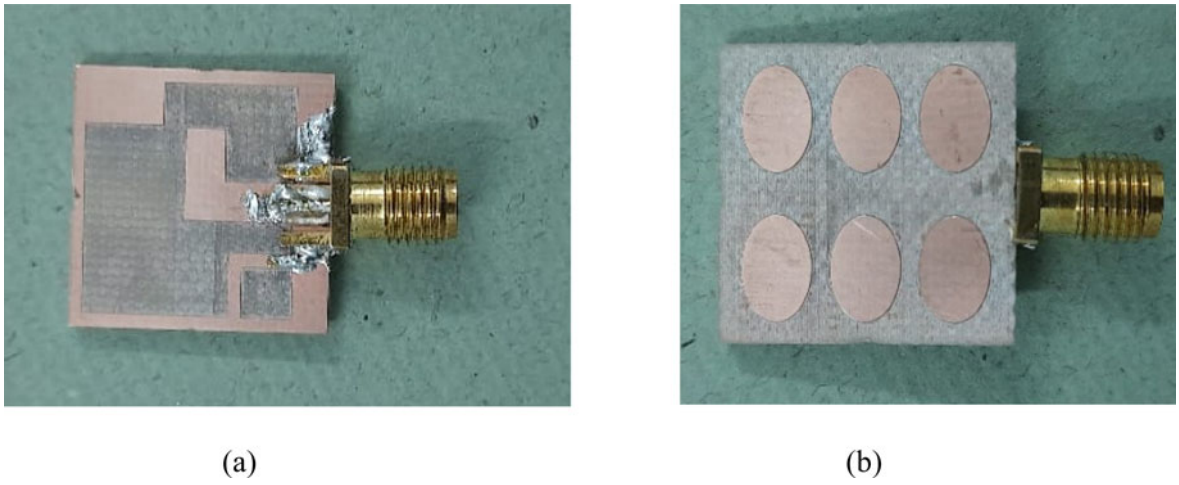


Fig. 15. (a) Top view and (b) bottom view of the proposed fabricated structure.

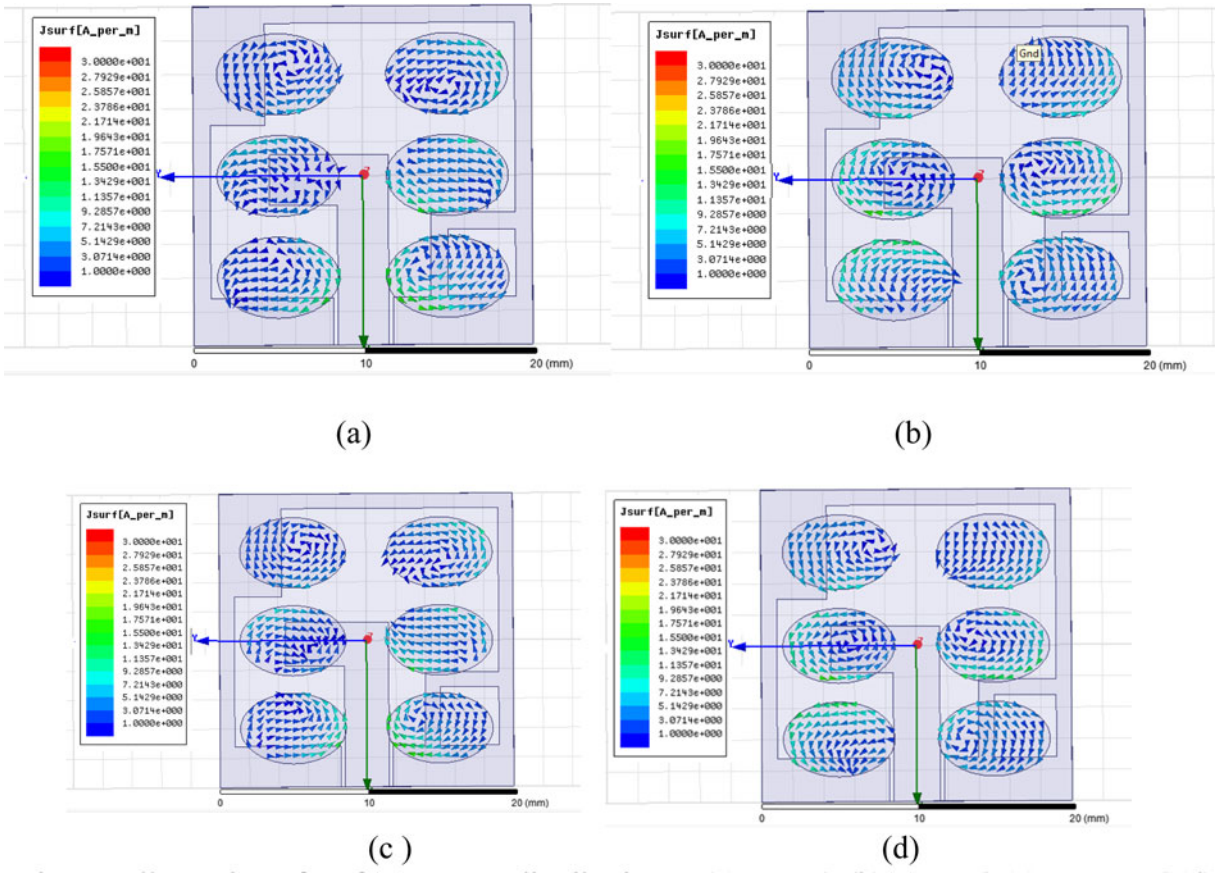


Fig. 16. Illustration of surface current distribution at $\omega t = 0°$, 90°, 180°, 270°.

i.e. 0.59 dB, is obtained when W_p attains a value of 3 mm, thus leading to the finalization of the value of W_p to 3 mm.

Parametric study on varying the length of patch, L_p

It is observed from Fig. 14 that the length of the patch is varied from 6 to 8 mm and the resonant frequency of the antenna shifts to the lower side of the frequency with the minimum frequency obtained at 4.49 GHz corresponding to L_p equal to 7 mm. The AR characteristic also improves at L_p equal to 7 mm. Thus, L_p is optimized to 7 mm.

Experimental results

The top and bottom views of the fabricated prototype of the proposed antenna which uses the Agilent vector analyzer (N5230A:

https://doi.org/10.1017/S1759078721001367 Published online by Cambridge University Press

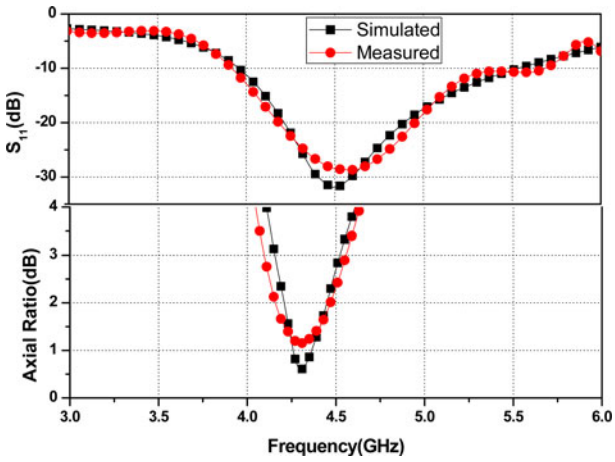


Fig. 17. Responses (measured and simulated) of S_{11} and axial ratio versus frequency.

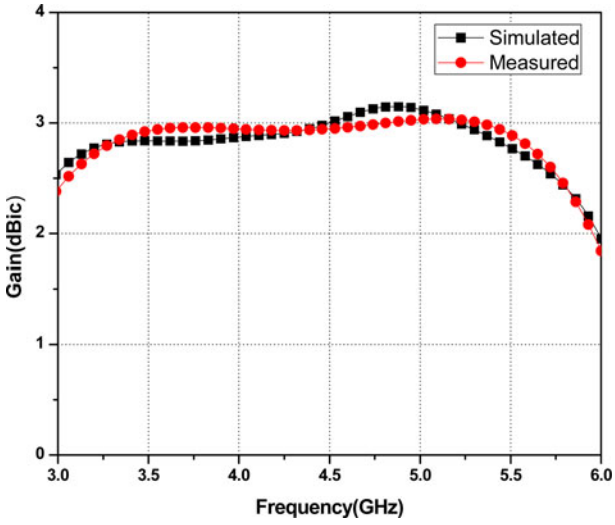


Fig. 18. Responses (measured and simulated) of gain versus frequency.

PNA-L) is depicted in Fig. 15. To know how CP waves are generated by the proposed antenna, the vector surface current distribution on the six EEBGs is analyzed by varying the phase at various time phases ($\omega t = 0°$, 90°, 180°, 270°). Figure 16 depicts that at $\omega t = 0°$ and 90°, the vector surface currents are of the same magnitude and is in phase opposition at $\omega t = 180°$ and 270°, respectively. This indicates that since there is change in the phase, the rotation of the simulated surface current vectors is in the anticlockwise direction, indicating that left hand circular polarization (LHCP) is achieved.

Figure 17 not only shows the measured results of S_{11}, but also compares the axial ratio versus frequency with the simulated results. It is depicted that the proposed antenna offers measured impedance bandwidth of 36.9% which lies in the range 3.91–5.68 GHz and shows a good agreement with the simulated result of 33.33% (3.95–5.53 GHz). The measured AR bandwidth of 9.98% (4.09–4.52 GHz) also matches well with the simulated result of 8.53% (4.15–4.52 GHz). A slight difference in the measured and simulated result may be present because of fabrication tolerance and errors occurring in the measurement system. It is also observed from Fig. 18 that upon implementation of the EEBG on the antenna, the simulated peak gain in the AR bandwidth is 3 dBic. This is attributed to the surface waves being prohibited by the EEBG which leads to the enhancement of the gain.

Figure 19 reveals the radiation characteristics of the proposed antenna in the *E* and *H* planes, respectively, at 4.33 GHz, depicting that in both the planes, LHCP waves are observed. Table 4 compares the proposed antenna with few of the reported CP antennas. From the evaluation of the comparison in Table 4, it is revealed that the proposed antenna is more compact with the impedance bandwidth and the AR bandwidth has improved as compared to the ones reported in Table 4.

Conclusion

An EEBG-based CP antenna which maneuvers at 4.3 GHz has been proposed in this paper. Using a 3 × 2 array EEBG on the substrate of the proposed antenna, an enhancement is observed in the antenna's performance with an impedance bandwidth of

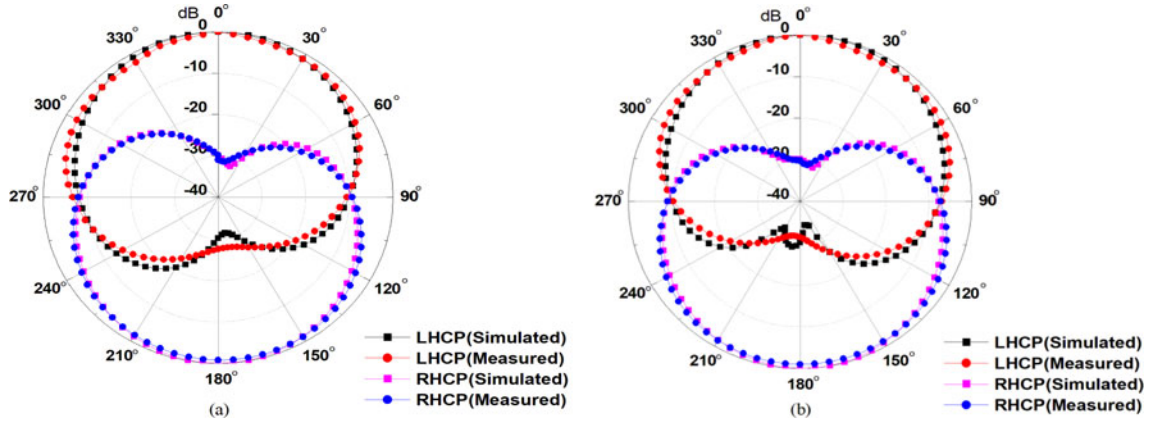


Fig. 19. Radiation pattern at 4.3 GHz: (a) *E*-plane and (b) *H*-plane.

https://doi.org/10.1017/S1759078721001367 Published online by Cambridge University Press

Table 4. Comparison table of reported CP antenna with our proposed antenna provided in the literature

Ref.	Overall size of antenna (mm^3)	Dielectric constant (ϵ_r)	Measured impedance bandwidth (GHz) (< −10 dB)	Measured AR bandwidth (GHz) (<3 dB)	Gain (dBic)	Techniques
[9]	35 × 35 × 3.7	4.4	2.47–2.60 (5.12%)	2.51–2.55 (1.6%)	3.41	CP antenna with RIS on substrate
[12]	117 × 117 × 4	4.1	1.681–1.841 (9.08%)	1.798–1.826 (1.54%)	4.2	CP antenna using EBG in ground plane
[15]	120 × 120 × 9.2	4.2	2.45–2.66 (8.20%)	2.46–2.53 (2.80%)	–	Slot antenna with metasurface used as a polarizer
[19]	60 × 60 × 4	10	1.55–1.62 (4.41%)	1.563–1.595 (2%)	4	CP antenna with fractal EBG in ground plane
[20]	109.5 × 109.5 × 1.2	4.4	2.349–2.477 (5.31%)	2.41–2.441 (1.28%)	–	Slot antenna with mushroom-shaped EBG surrounding the slot antenna
[23]	80 × 80 × 1.6	4.4	2.357–2.477 (4.97%)	2.375–2.425 (2.08%)	3.52	Polarization-dependent slot-loaded EBG surrounding rotated truncated square patch antenna
[24]	30 × 30 × 3.2	4.4	4.63–5.55 (18%)	4.94–5.27 (6.4%)	5.93	Hexagonal ring EBG on substrate of circular patch antenna with T slot
[29]	30 × 30 × 3.2	4.4	2.82–4.00 (34.6%)	3.13–3.35 (6.8%)	3.91	EBG-based metasurface on a slot antenna
Our work	20 × 20 × 1.5	4.4	3.91–5.68 (36.9%)	4.09–4.52 (9.98%)	3.0	CP antenna with elliptical EBG on the substrate

36.9%, an AR bandwidth of 9.98%, and a gain of 3 dBic, thus making this antenna a contender to be utilized for WAIC systems.

References

1. **Kan H and Waterhouse RB** (2000) Small circularly polarised printed antenna. *Electronics Letters* **36**, 393.
2. **Lam KY, Luk K, Lee KF, Wong H and Ng KB** (2011) Small circularly polarized u-slot wideband patch antenna. *IEEE Antennas and Wireless Propagation Letters* **10**, 87–90.
3. **Patil S, Singh AK, Kanaujia BK and Yadava RL** (2018) Design of inclined coupling slot loaded CPW-fed circularly polarized slot antenna for wireless applications. *Electromagnetics* **38**, 226–235.
4. **Singh AK, Patil S, Kanaujia BK and Pandey VK** (2020) A novel printed circularly polarized asymmetric wide slot antenna for digital cellular system. *Microwave and Optical Technology Letters* **6**, 1438–1447.
5. **Nasimuddin N, Qing X and Chen Z** (2010) Slits loaded microstrip antennas for circular polarization. *Microwave and Optical Technology Letters* **52**, 2043–2049.
6. **Patil S, Singh AK, Kanaujia BK and Yadava RL** (2017) Design of dual band dual sense circularly polarized wide slot antenna with C-shaped radiator for wireless applications. *Frequenz* **72**, 1–9.
7. **Singh AK, Gangwar RK and Kanaujia BK** (2016) Sectored annular ring microstrip antenna with DGS for circular polarization. *Microwave and Optical Technology Letters* **58**, 569–573.
8. **Thakur JP and Par JS** (2006) An advance design approach for circular polarization of the microstrip antenna with unbalance DGS feedlines. *IEEE Antennas and Wireless Propagation Letters* **5**, 101–103.
9. **Agarwal K and Nasimuddin AA** (2013) RIS-based compact circularly polarized microstrip antennas. *IEEE Transactions on Antennas and Propagation* **61**, 547–554.
10. **Zarrabi FB, Mansouri Z, Ahmadian R, Rahimi M and Kuhestani H** (2015) Microstrip slot antenna applications with SRR for WiMAX/WLAN with linear and circular polarization. *Microwave and Optical Technology Letters* **5**, 1332–1338.
11. **Dong Y, Toyao H and Itoh T** (2012) Design and characterization of miniaturized patch antennas loaded with complementary split-ring resonators. *IEEE Transactions on Antennas and Propagation* **60**, 772–785.
12. **Pflaum S, Philippe LT, Kossiavas G and Robert S** (2013) Performance enhancement of a circularly polarized patch antenna for radio frequency identification readers using an electromagnetic band-gap ground plane. *Microwave and Optical Technology Letters* **55**, 1599–1602.
13. **Sudha T and Vedavathy TS** (2002) A Dual Band Circularly Polarized Microstrip Antenna on an EBG Substrate. In: IEEE Antennas and Propagation Society International Symposium, 2002, 16–21 June, San Antonio, Texas, 2, 68–71.
14. **Rahman M and Stuchly MA** (2002) Circularly polarised patch antenna with periodic structure. *IEE Proceedings – Microwaves, Antennas and Propagation* **149**, 141–146.
15. **Zhu H, Chung KL, Sun XL, Cheung SW and Yuk TI** (2012) CP metasurfaced antennas excited by LP sources. *IEEE Transactions on Antennas and Propagation* **61**, 4615–4623.
16. **Yang F and Rahmat-Samii Y** (2005) A low profile single dipole antenna radiating circularly polarized waves. *IEEE Transaction on Antennas and Propagation* **50**, 3083–3086.
17. **Xiulong B, Ruvio G and Ammann MJ** (2008) A circularly polarized annular-ring patch antenna with a groundplane EBG annular-slot array. *International Journal of Microwave and Optical Technology* **3**, 69–75.
18. **Ahmed MF, Shaalan AH and Awadalla KH** (2015) design and simulation of a single fed multi-band circularly polarized microstrip antenna with slots progress. *Electromagnetics Research C* **57**, 71–79.
19. **Encheng W and Liu Q** (2016) GPS patch antenna loaded with fractal EBG structure using organic magnetic substrate progress. *Electromagnetics Research Letters* **58**, 23–28.
20. **Wang KY, Zhang Z, Hong B, Luo X and Guo Q** (2017) An axial-ratio beam-width enhancement of patch-slot antenna based on EBG. *Microwave and Optical Technology Letters* **59**, 493–497.

https://doi.org/10.1017/S1759078721001367 Published online by Cambridge University Press

21. **Da Silva JP, De Siqueira Campos ALP and De Andrade HD** (2018) Using metasurface structures as signal polarisers in microstrip antennas. *IET Microwaves, Antennas & Propagation* **13**, 23–27.
22. **Qi Z, Guo C, Vandenbosch GAE and Ding J** (2019) Low-profile circularly polarized array with gain enhancement and RCS reduction using polarization conversion EBG structures. *IEEE Transactions on Antennas and Propagation* **68**, 2440–2445.
23. **Verma A, Singh AK, Srivastava N, Patil S and Kanaujia BK** (2020) Circularly polarized microstrip antenna using SLPD electromagnetic bandgap structure. *Frequenz* **74**, 41–51.
24. **Verma A, Singh AK, Srivastava N, Patil S and Kanaujia BK** (2020) Hexagonal ring electromagnetic band gap based slot antenna for circular polarization and performance enhancement. *Microwave and Optical Technology Letters* **62**, 2576–2587.
25. **Wu Z, Li L, Li Y and Chen X** (2016) Metasurface superstrate antenna with wideband circular polarization for satellite communication application. *IEEE Antennas and Wireless Propagation Letters* **15**, 374–377.
26. **Sihao L, Deqiang Y and Jin P** (2019) A Low-profile circularly polarized metasurface antenna with wide axial-ratio beamwidth. *IEEE Antennas and Wireless Propagation Letters* **18**, 1438–1442.
27. **Zhipeng L, Ouyang J and Yang F** (2018) Low-profile wideband circularly polarized single-layer metasurface antenna. *Electronics Letters* **54**, 1362–1364.
28. **Hussain N and Parka MI** (2017) Design of a wide-gain-bandwidth metasurface antenna at terahertz frequency. *AIP Advances* **7**, 0553131–11.
29. **Verma A, Singh AK, Srivastava N, Patil S and Kanaujia BK** (2019) Slot loaded EBG-based metasurface for performance improvement of circularly polarized antenna for WiMAX applications. *International Journal of Microwave and Wireless Technologies* **12**, 212–220.
30. **Soumik D and Dey S** (2020) EBG Superstrate Loaded Circularly Polarized Fabry-Perot Cavity Antenna at Sub-6 GHz for Satellite and 5 G Cellular Communications, IEEE International Symposium on Antennas & Propagation (APSYM), 14–16 Dec. 2020, Cochin, India.
31. **Zeppettella D and Ali M** (2020) A broadband directional circularly polarized spiral antenna on EBG structure. *Journal of Electromagnetic Waves and Applications* **34**, 1–23.
32. **Samineni PT and De Khan A** (2016) Modeling of electromagnetic band gap structures: a review. *International Journal RF and Microwave Computer-Aided Engineering* **27**, 1–19.
33. **Sievenpiper D, Zhang L, Broas RFJ, Alexopolous NG and Yablonovitch E** (1999) High impedance electromagnetic surfaces with a forbidden frequency band. *IEEE Transactions on Microwave Theory and Techniques* **47**, 2059–2074.



Dr. Shilpee Patil received her B.Tech. degree in Electronics & Communication Engineering from AKTU (formerly UPTU), Lucknow, India, and her M.Tech. degree in Digital Communication from GGSIP University, Delhi, India, in 2009. She pursued her Ph.D. degree in Electronics Engineering from AKTU, Lucknow, India. Her research interests are microstrip antennas, slot antennas, and circularly polarized microstrip antennas.



Alka Verma received her B.E. degree in Electrical & Electronics from Bangalore University, Karnataka, India. She has completed her M.Tech. degree in Electronics Engineering from, Dr. A.P.J Abdul Kalam Technical University (formerly UPTU), Lucknow (U.P.), India and currently pursuing her Ph.D. degree from the same. Her areas of interests are microstrip antennas, electromagnetic band gap structures and circularly polarized microstrip antennas for wireless communications.



Dr. Anil Kumar Singh was born in Jamalpur, Mirzapur (U.P.), India in 1976. He has completed his M.Tech. degree in Instrumentation and Control Engineering from NITTTR Chandigarh, India and his Ph.D. degree on Studies on Annular Ring Microstrip Antenna for different Applications from Electronics Engineering Department, Indian School of Mines (ISM), Dhanbad, India. He joined the Department of Electronics and Instrumentation Engineering, Institute of Engineering and Technology, M. J. P. Rohilkhand University, Bareilly as a lecturer in 2002. He has published more than 20 papers in national and international journals and conferences. His current research interest includes design and analysis of microstrip antennas.



Dr. Binod Kumar Kanaujia is working as Professor in the School of Computational and Integrative Sciences, Jawaharlal Nehru University, New Delhi since August 2016. Dr. Kanaujia completed his B.Tech. in Electronics Engineering from KNIT, Sultanpur, India in 1994. He obtained his M.Tech. and Ph.D. in 1998 and 2004, respectively, from the Department of Electronics Engineering, I.I.T. B.H.U., Varanasi, India. He has a keen research interest in design and modeling of reconfigurable and circular polarized microstrip antennas. He has been credited to publish more than 150 research papers with more than 430 citations with an *h*-index of 12 in peer-reviewed journals and conferences. He successfully executed 4 research projects sponsored by several agencies of Government of India .e.g. DRDO, DST, AICTE, and ISRO. He is a member of several academic and professional bodies e.g. IEEE, Institution of Engineers (India), Indian Society for Technical Education and Institute of Electronics and Telecommunication Engineers of India.



Dr. Suresh Kumar is working as an Associate Professor in the Department of Computer Science and Engineering in Netaji Subhas University and Technology, Delhi. He has a teaching experience of more than 15 years. He has completed his M.Sc. in Computer Science from KUK, Kurukshetra, India. He obtained his M.Tech. in Computer Science and Engineering from KUK, Kurukshetra, India and his Ph.D. from MDU, Rohtak, India. He has a keen research interest in database management system, operating system, Semantic Web, etc. He has published 12 research papers in peer-reviewed international journals and seven papers in international conferences.

https://doi.org/10.1017/S1759078721001367 Published online by Cambridge University Press